Unified theory of structures based on micropolar elasticity

Unified theory of structures based on micropolar elasticity

R. Augello*, E. Carrera†, A. Pagani‡

Mul^2 Group
Department of Mechanical and Aerospace Engineering, Politecnico di Torino
Corso Duca degli Abruzzi 24, 10129 Torino, Italy.

Abstract: *This paper intends to establish a unified theory of structures based on the Micropolar Elasticity (ME). ME allows taking into consideration the microstructure of the material, through the adoption of four additional material parameters. In this way, the size-effects of the structure can be caught. The proposed model is developed in the domain of the Carrera Unified Formulation (CUF), according to which theories of structures can degenerate into unknown kinematics that makes use of an arbitrary expansion of the generalized variables. CUF is a hierarchical formulation that considers the order of the structural model as input of the analysis, so that no specific approximation and manipulation is needed to implement refined theories. Different types of structures have been analyzed in the present work, and the results are compared and validated with benchmarks from the literature. The effects of the new material parameters are addressed too, along with the capability of the proposed model to deal with size-effects and high-order structural behaviors. Finally, stress analysis is detailed to further highlight the differences between micropolar and classical elasticity.*

Keywords: Micropolar elasticity; Unified theory; Refined model

1 Introduction

In engineering and scientific applications, the classical continuum mechanics represents the most adopted tool to analyse structural problems. Based on classical elasticity, many reliable engineering structural theories have been formulated over the centuries, see for example the Euler-Bernoulli [1] or Timoshenko bending theories [2] and the Coulomb torsion theory [3], extended to prisms of any shape by Saint-Venant [4]. These theories have produced acceptable results for various applications. Classical Elasticity (CE) assumes that the rotations within the continuum are a direct consequence of displacements and the interaction between adjacent points occur only by means of translational forces. However, in many cases, it may no longer represent an appropriate and reliable mathematical model to describe the physical phenomena that happen within the structure. Kennedy [5] showed how CE cannot accurately describe large stress gradients in the proximity of holes, analyzing notched plates with circular

*Post Graduate Research Assistant. E-mail: riccardo.augello@polito.it
†Professor of Aerospace Structures and Aeroelasticity
‡Assistant Professor. Corresponding author. E-mail: alfonso.pagani@polito.it

and elliptical holes and the strain-softening of the material at the notch. Besides, when the size of the analysed structure is comparable to the microstructural scale, the body behaves quite differently from the prediction that CE could lead to. As an example, this behavior is evident when dealing with Micro-Electro Mechanical System (MEMS) and Nano-Electro Mechanical System (NEMS) devices. Li *et al.* [6] highlighted the need to perform an appropriate micromechanical and nanomechanical characterization (through nanoindentation techniques) to evaluate the mechanical properties of structures with micro and nano size. In these cases, the microstructure of the material must be considered, as demonstrated by the experimental research conducted by McFarland and Colton [7], and by Lam et al. [8]. Moreover, one of the main advantages of ME is due to its regularization properties in physically nonlinear problems (elasto-plasticity and damage) where localization occurs (see Peerlings *et al.* [9]).
To overcome the problems that arise when adopting CE in the aforementioned cases, several generalized continua models have been developed; e.g., see Kunin [10, 11]. For a comprehensive review of the generalized continuum theories developed in history, interested readers can refer to Maugin and Metrikine [12]. Among the generalized continuum theories, Micropolar Elasticity (ME) deserves particular attention. At the end of the 19th century, the main ideas leading to the micropolar continuum (and, in general, to the other generalized media models), were discussed by many authors. One of the most important work is the one made by Voigt [13], who suggested that the interaction of two parts of the body is transmitted not only through a translational force but also through a moment. The complete theory of asymmetric elasticity was further developed by the brothers François and Eugène Cosserat [14], who introduced the asymmetry of the force-stress tensor and deformations tensor. In addition, every particle of the material is meant to be able to rotate independently of the surrounding particles, and so additional unknown rotations are needed to describe the motion. As a consequence, every particle has six degrees of freedom, three translations associated with the macrostructure, and three rotations, associated with the microstructure. The theory was further developed by Eringen [15, 16, 17] , who gave it the name Micropolar Elasticity, and Nowacki [18, 19]. The asymmetry of the stresses and deformations tensors is achieved by ME through the addition of four material parameters, which represents the contribution that the microstructure has on the behavior of the structure at the macro-scale. The identification of these material parameters is difficult to be performed by numerical simulation, and it is limited to experimental research. See for example the work conducted on bones with torsion and bending by Yang and Lakes [20], on notched bones by Lakes *et al.* [21] and on a polymeric foam by Lakes [22]. A review of the experiments conducted to micropolar materials has been done by Hassanpour and Heppler [23], who also proposed some numerical and analytical methods for the evaluation of the additional material parameters through homogenization procedure.
There are some examples in the literature about the application of structural theories based on ME. Huang *et al.* [24] developed a bending model for the analysis of beams, considering the material as a micropolar one. This work made use of Euler-Bernoulli theory and the Finite Element Method (FEM) to study the effects of the additional material parameters of ME on the bending behavior of beams. Ramezani *et al.* [25] showed a bending model based on the linear theory of beams based on micropolar continuum mechanics. In their work, the Timoshenko First-Order Shear Deformation Beam Theory (FSDBT) was used, and the microrotation was considered constant over the cross-section but different from the bending rotation of the structure. Besides the bending theory, the torsional behavior of micropolar beam model was analyzed by Hassanpour and Heppler [26], who developed a beam model able to take into account both bending (based on Timoshenko theory) and torsional effects

(based on an extended form of Duleau torsion theory). To evaluate local effects and thickness and cross-section deformations, higher-order models were developed, for example, by Zozulya [27, 28], who generated higher-order models for plates, shells and curved rods.
The purpose of this paper is to develop a unified structural theory based on ME. The framework in which the proposed methodology is developed is the Carrera Unified Formulation (CUF), according to which the unknowns field can be expressed as an arbitrary expansion of the generalized variables. As a consequence, the theory of structure is considered as an input of the analysis, so there is no need for an *ad hoc* implementation to obtain refined models. In fact, any higher-order theory is obtained by means of the so-called fundamental nucleus (FN), that represents the basic building blocks which can be expanded in an arbitrary way. In recent years, CUF has explored various engineering problems, including thin-walled cross-section beams by Carrera and Varello [29], post-buckling by Fazzolari and Carrera [30] and geometrical nonlinearity for both metallic and composite structures by Pagani and Carrera [31, 32], among the others. Many engineering fields have been investigated, such as civil by Carrera and Pagani [33], aerospace by Carrera *et al.* [34] and multi-field by Miglioretti and Carrera [35]. Recently, Carrera and Zozulya [36] developed an analytical solution based on CUF and ME. In the present work, the formulation is further extended to make use of finite element analysis and thus to deal with arbitrary boundary conditions, geometry and loadings.
This paper is organized as follows: (i) first, ME is briefly introduced in Section 2, and the strain-displacement and constitutive relations are written in a unified manner; (ii) subsequently, in Section 3, the evaluation of the FN of the stiffness matrix is shown.; (iii) then, in Section 4, numerical results are discussed and some comparisons with the results from the literature are reported. Three-dimensional distribution of the stress field is addressed too; (iv) finally, the main conclusions are drawn. Furthermore, appendix sections are provided, and they give the components of the stiffness matrix.

2 Unified micropolar beam element

2.1 Preliminaries

Consider a beam structure whose cross-section Ω lays on the xz-plane of a Cartesian reference system. As a consequence, the beam axis is placed along y and measures L. The transposed unknowns vector is introduced in the following:

$$\mathbf{u}(x,y,z) = \left\{ \begin{array}{cccccc} u_x & u_y & u_z & \omega_x & \omega_y & \omega_z \end{array} \right\}^T \tag{1}$$

where u represents displacements and ω represents micro-rotations. The force stress $\boldsymbol{\sigma}$, micropolar couple stress $\boldsymbol{\mu}$, strain $\boldsymbol{\epsilon}$ and twist $\boldsymbol{\chi}$ components are expressed in vectorial form,

$$\begin{aligned}
\boldsymbol{\sigma} &= \left\{ \begin{array}{cccccccccc} \sigma_{xx} & \sigma_{yy} & \sigma_{zz} & \sigma_{xy} & \sigma_{yx} & \sigma_{xz} & \sigma_{zx} & \sigma_{yz} & \sigma_{zy} \end{array} \right\}^T \\
\boldsymbol{\epsilon} &= \left\{ \begin{array}{cccccccccc} \epsilon_{xx} & \epsilon_{yy} & \epsilon_{zz} & \epsilon_{xy} & \epsilon_{yx} & \epsilon_{xz} & \epsilon_{zx} & \epsilon_{yz} & \epsilon_{zy} \end{array} \right\}^T \\
\boldsymbol{\mu} &= \left\{ \begin{array}{cccccccccc} \mu_{xx} & \mu_{yy} & \mu_{zz} & \mu_{xy} & \mu_{yx} & \mu_{xz} & \mu_{zx} & \mu_{yz} & \mu_{zy} \end{array} \right\}^T \\
\boldsymbol{\chi} &= \left\{ \begin{array}{cccccccccc} \chi_{xx} & \chi_{yy} & \chi_{zz} & \chi_{xy} & \chi_{yx} & \chi_{xz} & \chi_{zx} & \chi_{yz} & \chi_{zy} \end{array} \right\}^T
\end{aligned} \tag{2}$$

In this work, linear elastic metallic structures are considered. Hence, Hooke's law providing the constitutive relation holds as follows (see Ref. [27]) is, in a tensorial form:

$$\boldsymbol{\sigma} = \lambda(tr\boldsymbol{\epsilon})\mathbf{I} + (\mu+\alpha)\boldsymbol{\epsilon} + (\mu-\alpha)\boldsymbol{\epsilon}^T, \qquad \boldsymbol{\mu} = \beta(tr\boldsymbol{\chi})\mathbf{I} + (\gamma+\epsilon)\boldsymbol{\chi} + (\gamma-\epsilon)\boldsymbol{\chi}^T \tag{3}$$

or, analogously,

$$\boldsymbol{\sigma} = \mathbf{C}\boldsymbol{\epsilon}, \qquad \boldsymbol{\mu} = \mathbf{A}\boldsymbol{\chi} \tag{4}$$

where the material matrix $\mathbf{C}$ is

$$\mathbf{C} = \begin{bmatrix} C_{11} & C_{12} & C_{13} & 0 & 0 & 0 & 0 & 0 & 0 \\ C_{12} & C_{22} & C_{23} & 0 & 0 & 0 & 0 & 0 & 0 \\ C_{13} & C_{23} & C_{33} & 0 & 0 & 0 & 0 & 0 & 0 \\ 0 & 0 & 0 & C_{44}^{M} & C_{44}^{MT} & 0 & 0 & 0 & 0 \\ 0 & 0 & 0 & C_{44}^{MT} & C_{44}^{M} & 0 & 0 & 0 & 0 \\ 0 & 0 & 0 & 0 & 0 & C_{55}^{M} & C_{55}^{MT} & 0 & 0 \\ 0 & 0 & 0 & 0 & 0 & C_{55}^{MT} & C_{55}^{M} & 0 & 0 \\ 0 & 0 & 0 & 0 & 0 & 0 & 0 & C_{66}^{M} & C_{66}^{MT} \\ 0 & 0 & 0 & 0 & 0 & 0 & 0 & C_{66}^{MT} & C_{66}^{M} \end{bmatrix} \tag{5}$$

and

$$\begin{aligned} C_{11} = C_{22} = C_{33} &= \lambda + 2\mu, \\ C_{12} = C_{13} = C_{23} &= \lambda, \\ C_{44}^{M} = C_{55}^{M} = C_{66}^{M} &= \mu + \alpha, \\ C_{44}^{MT} = C_{55}^{MT} = C_{66}^{MT} &= \mu - \alpha \end{aligned} \tag{6}$$

with λ and μ being Lamé constants of classical elasticity, and α micropolar constant. The matrix $\mathbf{A}$ in Eq. (4) is:

$$\mathbf{A} = \begin{bmatrix} A_{11} & A_{12} & A_{13} & 0 & 0 & 0 & 0 & 0 & 0 \\ A_{12} & A_{22} & A_{23} & 0 & 0 & 0 & 0 & 0 & 0 \\ A_{13} & A_{23} & A_{33} & 0 & 0 & 0 & 0 & 0 & 0 \\ 0 & 0 & 0 & A_{44}^{M} & A_{44}^{MT} & 0 & 0 & 0 & 0 \\ 0 & 0 & 0 & A_{44}^{MT} & A_{44}^{M} & 0 & 0 & 0 & 0 \\ 0 & 0 & 0 & 0 & 0 & A_{55}^{M} & A_{55}^{MT} & 0 & 0 \\ 0 & 0 & 0 & 0 & 0 & A_{55}^{MT} & A_{55}^{M} & 0 & 0 \\ 0 & 0 & 0 & 0 & 0 & 0 & 0 & A_{66}^{M} & A_{66}^{MT} \\ 0 & 0 & 0 & 0 & 0 & 0 & 0 & A_{66}^{MT} & A_{66}^{M} \end{bmatrix} \tag{7}$$

where,

$$\begin{aligned} A_{11} = A_{22} = A_{33} &= \beta + 2\gamma, \\ A_{12} = A_{13} = A_{23} &= \beta, \\ A_{44}^{M} = A_{55}^{M} = A_{66}^{M} &= \gamma + \epsilon, \\ A_{44}^{MT} = A_{55}^{MT} = A_{66}^{MT} &= \gamma - \epsilon \end{aligned} \tag{8}$$

with β, γ and ϵ being additional micropolar elastic constant (see Ref. [27]).
The kinematic relations are expressed as:

$$\boldsymbol{\epsilon} = (\mathbf{b}_{m1})\mathbf{u}, \qquad \boldsymbol{\chi} = (\mathbf{b}_{m2})\mathbf{u} \tag{9}$$

where $\mathbf{b}_{m1}$ and $\mathbf{b}_{m2}$ are the differential operators:

$$\mathbf{b}_{m1} = \begin{bmatrix} \partial_x & 0 & 0 & 0 & 0 & 0 \\ 0 & \partial_y & 0 & 0 & 0 & 0 \\ 0 & 0 & \partial_z & 0 & 0 & 0 \\ \partial_y & 0 & 0 & 0 & 0 & 1 \\ 0 & \partial_x & 0 & 0 & 0 & -1 \\ \partial_z & 0 & 0 & 0 & -1 & 0 \\ 0 & 0 & \partial_x & 0 & 1 & 0 \\ 0 & \partial_z & 0 & 1 & 0 & 0 \\ 0 & 0 & \partial_y & -1 & 0 & 0 \end{bmatrix}, \qquad \mathbf{b}_{m2} = \begin{bmatrix} 0 & 0 & 0 & \partial_x & 0 & 0 \\ 0 & 0 & 0 & 0 & \partial_y & 0 \\ 0 & 0 & 0 & 0 & 0 & \partial_z \\ 0 & 0 & 0 & \partial_y & 0 & 0 \\ 0 & 0 & 0 & 0 & \partial_x & 0 \\ 0 & 0 & 0 & \partial_z & 0 & 0 \\ 0 & 0 & 0 & 0 & 0 & \partial_x \\ 0 & 0 & 0 & 0 & \partial_z & 0 \\ 0 & 0 & 0 & 0 & 0 & \partial_y \end{bmatrix} \tag{10}$$

where $\partial_x = \dfrac{\partial(\cdot)}{\partial x}$, $\partial_y = \dfrac{\partial(\cdot)}{\partial y}$, and $\partial_z = \dfrac{\partial(\cdot)}{\partial z}$.

2.2 Higher-order unified Micropolar beam model

Within the framework of the Carrera Unified Formulation (CUF), the three-dimensional displacement field $\mathbf{u}(x, y, z)$ can be expressed as a general expansion of the primary unknowns, see Carrera et al. [37]. In the case of one-dimensional theories, one has:

$$\mathbf{u}(x, y, z) = F_s(x, z)\mathbf{u}_s(y), \qquad s = 1, 2, ..., M \tag{11}$$

where F_s are the functions of the coordinates x and z on the cross-section, $\mathbf{u}_s$ is the vector of the *generalized* displacements which lay along the beam axis, M stands for the number of the terms used in the expansion, and the repeated subscript s indicates summation. The choice of F_s determines the class of the 1D CUF model that is required and subsequently to be adopted. This notation is further discussed in Appendix A.

In this work, Lagrange Expansion (LE) beam theories based on CUF are employed (see Carrera et al. [38]). According to LE, piece-wise, and eventually higher-order, Lagrange polynomials are used as F_s to approximate the displacement and micro-rotation fields on the cross-section. Over the years, LE models have been demonstrated to provide reliable results for many applications, see for example [39, 33].

CUF has shown its capabilities in dealing with ME in the work made by Carrera and Zozulya [36], where an analytical solution of higher-order micropolar beam is proposed in a unified manner. In this work, instead, FEM is adopted to discretize the structure along the y axis. Thus, the generalized displacement vector $\mathbf{u}_s(y)$ is approximated as follows:

$$\mathbf{u}_s(y) = N_j(y)\mathbf{q}_{sj} \qquad j = 1, 2, \ldots, p+1 \tag{12}$$

where N_j stands for the j-th shape function, p is the order of the shape functions and j indicates summation. $\mathbf{q}_{sj}$ is the following vector of the FE nodal parameters:

$$\mathbf{q}_{sj} = \left\{ \begin{array}{cccccc} q_{u_{x_{sj}}} & q_{u_{y_{sj}}} & q_{u_{z_{sj}}} & \omega_{z_{sj}} & \omega_{z_{sj}} & \omega_{z_{sj}} \end{array} \right\}^T \tag{13}$$

For the sake of brevity, the shape functions N_j are not reported here. They can be found for instance in Bathe [40] and in Carrera *et al.* [37]. It should be underlined that the choice of the cross-section polynomials sets for the LE kinematics (i.e. the selection of the type, the number and the distribution of cross-sectional polynomials) is completely independent of the choice of the beam Finite Element (FE) to be used along the beam axis. In this work, classical one-dimensional FEs with four nodes (B4) are adopted, i.e. a cubic approximation along the y axis is assumed.

3 Fundamental nucleus of the micropolar FE stiffness matrix

The equilibrium equations of an elastic body can be obtained with ease by using the principle of virtual work:

$$\delta L_{\text{int}} = \delta L_{\text{ext}} \tag{14}$$

where L_{int} stands for the strain energy, L_{ext} is the work of the external loads, and δ represents the virtual variation. Given the stress ($\boldsymbol{\sigma}$), couple stress ($\boldsymbol{\mu}$), strain ($\boldsymbol{\epsilon}$) and twist ($\boldsymbol{\chi}$) vectors as in Eq. (2), the virtual variation of the internal strain energy can be written as

$$\delta L_{\text{int}} = \int_V \left((\delta \boldsymbol{\epsilon}^T \boldsymbol{\sigma}) + (\delta \boldsymbol{\chi}^T \boldsymbol{\mu}) \right) \, dV \tag{15}$$

$V = \Omega \times L$ is the volume of the beam structure. Introducing CUF (Eq. (11)) and FEM (Eq. (12) relations into Eq. (9), the strain and twist vectors can be written in algebraic form as follows:

$$\boldsymbol{\epsilon} = (\mathbf{B}_{m1}^{sj})\mathbf{q}_{sj}, \qquad \boldsymbol{\chi} = (\mathbf{B}_{m2}^{sj})\mathbf{q}_{sj} \tag{16}$$

where $\mathbf{B}_{m1}^{sj}$ and $\mathbf{B}_{m2}^{sj}$ are the following algebraic matrices:

$$\mathbf{B}_{m1}^{sj} = \mathbf{b}_{m1}(F_s\, N_j) = \begin{bmatrix} F_{s,x}N_j & 0 & 0 & 0 & 0 & 0 \\ 0 & F_sN_{j,y} & 0 & 0 & 0 & 0 \\ 0 & 0 & F_{s,z}N_j & 0 & 0 & 0 \\ F_sN_{j,y} & 0 & 0 & 0 & 0 & F_sN_j \\ 0 & F_{s,x}N_j & 0 & 0 & 0 & -F_sN_j \\ F_{s,z}N_j & 0 & 0 & 0 & -F_sN_j & 0 \\ 0 & 0 & F_{s,x}N_j & 0 & F_sN_j & 0 \\ 0 & F_{s,z}N_j & 0 & F_sN_j & 0 & 0 \\ 0 & 0 & F_sN_{j,y} & -F_sN_j & 0 & 0 \end{bmatrix} \tag{17}$$

$$\mathbf{B}_{m2}^{sj} = \mathbf{b}_{m2}(F_s\, N_j) = \begin{bmatrix} 0 & 0 & 0 & F_{s,x}N_j & 0 & 0 \\ 0 & 0 & 0 & 0 & F_sN_{j,y} & 0 \\ 0 & 0 & 0 & 0 & 0 & F_{s,z}N_j \\ 0 & 0 & 0 & F_sN_{j,y} & 0 & 0 \\ 0 & 0 & 0 & 0 & F_{s,x}N_j & 0 \\ 0 & 0 & 0 & F_{s,z}N_j & 0 & 0 \\ 0 & 0 & 0 & 0 & 0 & F_{s,x}N_j \\ 0 & 0 & 0 & 0 & F_{s,z}N_j & 0 \\ 0 & 0 & 0 & 0 & 0 & F_sN_{j,y} \end{bmatrix} \tag{18}$$

Substituitting Eq. (16) and the constitutive equations for elastic materials (Eq. (3)) into Eq. (15), one has:

$$\begin{aligned} \delta L_{\text{int}} &= \delta\mathbf{q}_{\tau i}^T \int \left((\mathbf{B}_{m1}^{\tau i})^T \mathbf{C} (\mathbf{B}_{m1}^{sj}) + (\mathbf{B}_{m2}^{\tau i})^T \mathbf{A} (\mathbf{B}_{m2}^{sj}) \right) dV\ \mathbf{q}_{sj} \\ &= \delta\mathbf{q}_{\tau i}^T\, \mathbf{K}^{ij\tau s}\, \mathbf{q}_{sj} \end{aligned} \tag{19}$$

where $\mathbf{K}^{ij\tau s}$ is the stiffness matrix. This matrix is given in terms of *fundamental nucleus*, which consists in a 6×6 matrix that, given the theory approximation order i.e., given the

cross-sectional functions ($F_\tau = F_s$, for $\tau = s$) and the shape functions ($N_i = N_j$, for $i = j$), can be expanded by using the indexes $\tau, s = 1, ..., M$ and $i, j = 1, ..., p+1$ in order to obtain the element stiffness matrices of any arbitrarily refined beam model. In other words, by opportunely choosing the beam kinematics, classical to higher-order beam theories and related stiffness array can be implemented in an automatic manner by exploiting the index notation of CUF. The expression of the matrix in Eq. (19) is given in Appendix A.

4 Numerical results

4.1 Assessment

The capability of the proposed unified theory of structure based on ME is demonstrated by the comparison with literature results. In the first analysis case, a cantilever, rectangular cross-section beam undergoing a vertical loading was considered. The reference solution of this analysis case comes from the work by Ramezani [25]. The beam is made by an isotropic

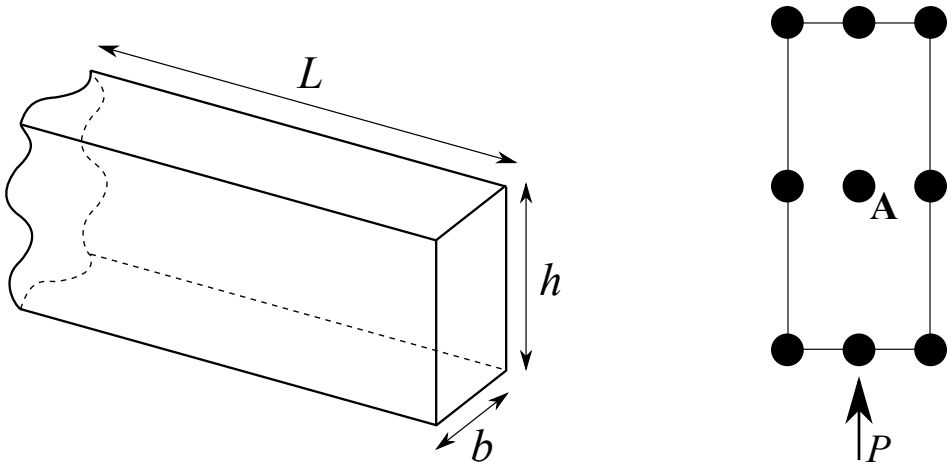

(a) (b)

Figure 1: Geometric properties (a), loading condition and LE cross-section model (b) for the first analysis case.

material with Young modulus $E = 20$ GPa and Poisson modulus $\nu = 0.3$. The values of the additional micropolar material parameters are those adopted in the reference paper, i.e. $\alpha = \dfrac{G}{40}$ and $\epsilon = \gamma = \dfrac{G}{10^4}$. Due to the different form of the constitutive relations between the present work and the reference one, the value of the β parameter is missing. However, static analyses were conducted with various values of the β and the results did not show any dependency from that value. Figure 1(a) shows the geometric conditions of the beam, where the aspect ratio L/h is equal to 10, and the aspect ratio of the cross-section h/b is equal to 4. One nine-node L9 Lagrange polynomial were adopted to discretize the cross-section as shown in Fig. 1(b). A preliminary convergence analysis was conducted to demonstrate the stability of the proposed FE approach when applied to Micropolar Elasticity (ME). Figure 2 shows non-dimensional displacements and micro-rotations for different mesh sizes and B4 beam elements. For all the cases considered, 10 B4 elements sufficed to meet convergence. Nevertheless, it is well known that FEs can be affected by instabilities and locking phenomena

in the case of ME and further assessment will be made in a future dedicated work. Figure 3

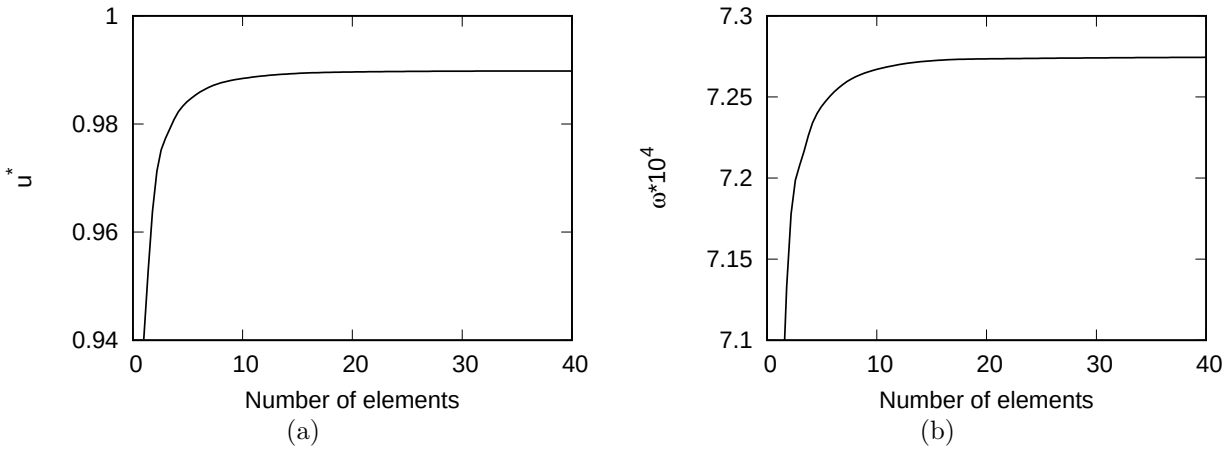

Figure 2: Convergence analysis of B4 FEs on the non-dimensional displacement (a) and micro-rotation (b) at the free edge of the beam. $u^* = \dfrac{3EIu(y)}{FL^3}$

shows the static results of the displacement and micro-rotation of point A (see Fig. 1(b)) obtained by the proposed model and by the reference paper. The results match both in terms of displacement and micro-rotation, although there is an oscillatory behavior from the reference solution, that has no physical meanings, as also revealed by Hassanpour and Heppler [26]. Finally, in Fig. 3(a), the solution obtained using the present LE and classical elasticity is illustrated, to highlight the difference from the ME.

The second numerical result deals with a comparison with the results obtained by Hassanpour and Heppler [26]. A cantilever, square cross-section beam was analyzed, but in this analysis case, the clamped unknowns were only the displacements, while the micro-rotations were set free. The geometric properties and the loading condition are shown in Fig. 4, along with the discretization adopted (one L9 Lagrange polynomial) over the cross-section. The material properties are the following, $\dfrac{\alpha}{E} = 10^{-2}$, $\dfrac{\gamma}{E} = \dfrac{\epsilon}{E} = 2.5 \times 10^{-4}$, $\dfrac{P}{EA} = 5 \times 10^{-6}$, and $\dfrac{L}{\sqrt{\dfrac{I}{A}}} = 10$, where A is the area of the cross-section. The static solutions using both CE and ME are shown in Fig. 5(a), where circles represent the solution proposed by the reference paper, and it can be seen that the results offered by the present paper follow the reference trend with high accuracy. In Fig. 5(b), the trend of the micro-rotations is shown. It is important to note that the micro-rotation in the clamped zone is not null because only the displacement variables are set to zero. It can be seen that the trend of the solution from the reference paper is reproduced by the present model. Note that the reference solution is based on the Timoshenko theory, while the present solution refers to an higher-order theory, so the slight discrepancy between the two solutions is due to the deformation of the cross-section, which cannot be taken into account from the reference model.

As an additional analysis, the trend of the normal and shear stress components is proposed in the following. Non-dimensional values of $\sigma_{YY}\ h^2/P$ and $\sigma_{YZ}\ h^2/P$ were evaluated along the thickness of three cross-sections of the beam, at the clamped zone ($y = 0.1L$), at the mid-span of the beam ($y = 0.5L$) and at the free end ($y = 0.9L$). Table 1 shows the values of the axial stress component and the same values are reported in Fig. 6. The values from the

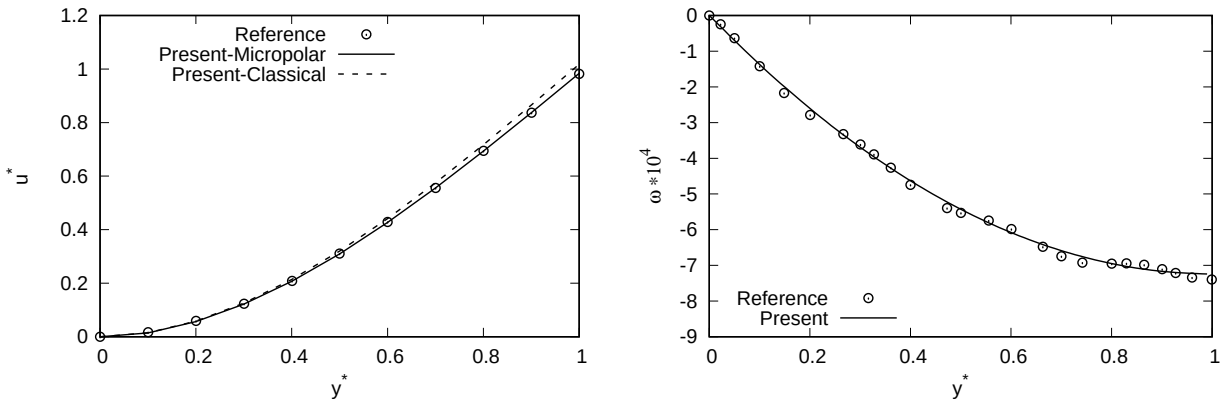

(a) (b)

Figure 3: Non-dimensional displacement ($u^* = \dfrac{3EIu(y)}{FL^3}$) over non-dimensional coordinate ($y^* = \dfrac{y}{L}$) (a) and micro-rotations [rad] over non-dimensional coordinate (b). Present results are compared to the ones from Ramezani [25] and to the results using CE. $\alpha = \dfrac{G}{40}$ and $\epsilon = \gamma = \dfrac{G}{10^4}$.

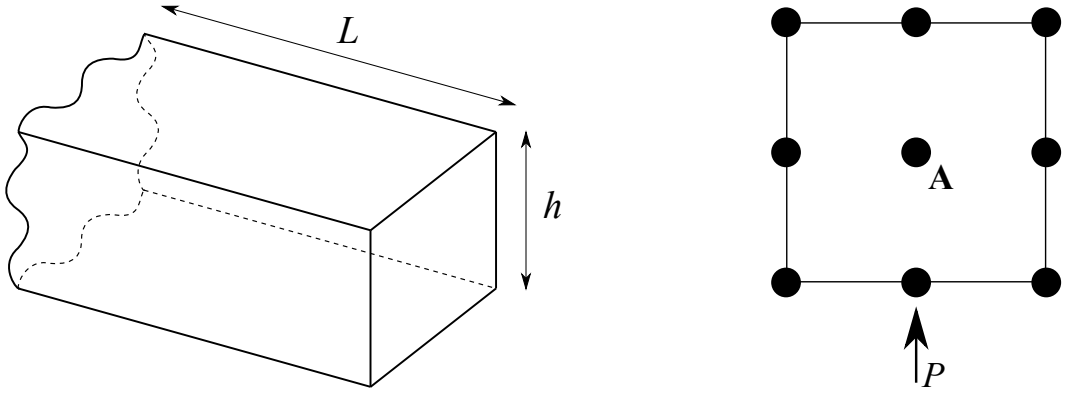

(a) (b)

Figure 4: Geometric properties (a), loading condition and LE cross-section model (b) for the second analysis case.

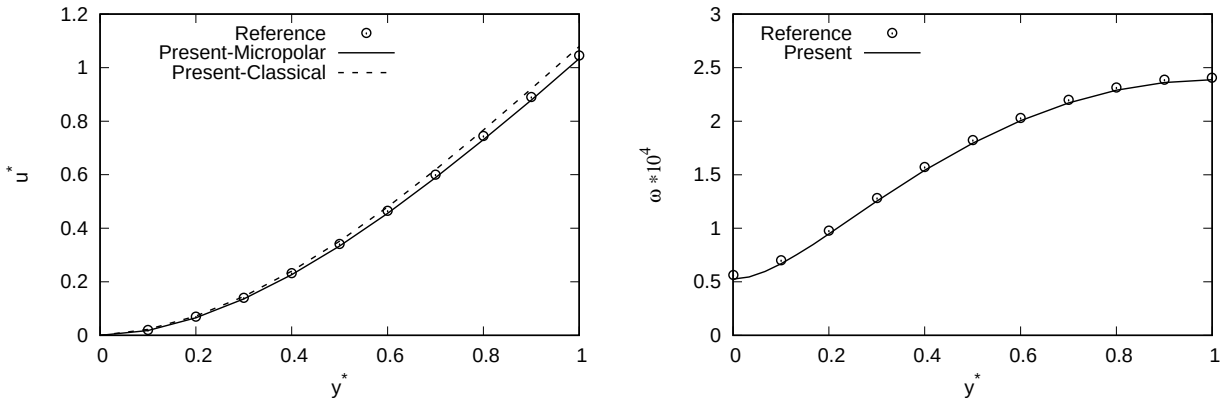

(a) (b)

Figure 5: Non-dimensional displacement ($u^* = \dfrac{3EILu(y)}{FAL^2}$) over non-dimensional coordinate ($y^* = \dfrac{y}{L}$) (a) and micro-rotations [rad] over non-dimensional coordinate (b). Present results are compared to the ones from Ramezani [26] and to the results using CE. $\dfrac{\alpha}{E} = 10^{-2}$, $\dfrac{\gamma}{E} = \dfrac{\epsilon}{E} = 2.5 \times 10^{-4}$.

	$\sigma_{YY}\ h^2/P$					
	y=0		y=0.5L		y=L	
z/h	CE	ME	CE	ME	CE	ME
0.500	15.28	14.88	8.663	8.259	1.938	1.841
0.333	10.19	9.920	5.775	5.506	1.292	1.227
0.167	5.090	4.960	2.888	2.735	0.646	0.614
0.000	0.000	0.000	0.000	0.000	0.000	0.000
-0.167	-5.090	-4.960	-2.888	-2.735	-0.646	-0.614
-0.333	-10.19	-9.920	-5.775	-5.506	-1.292	-1.227
0.500	-15.28	-14.88	-8.663	-8.259	-1.938	-1.841

Table 1: Values of the axial stress $\sigma_{YY}\ h^2/P$ component adopting both CE and ME solutions along the non-dimensional thickness z/h of three cross-section of the beam. 1L9 LE model. $\dfrac{\alpha}{E} = 10^{-2}$, $\dfrac{\gamma}{E} = \dfrac{\epsilon}{E} = 2.5 \times 10^{-4}$.

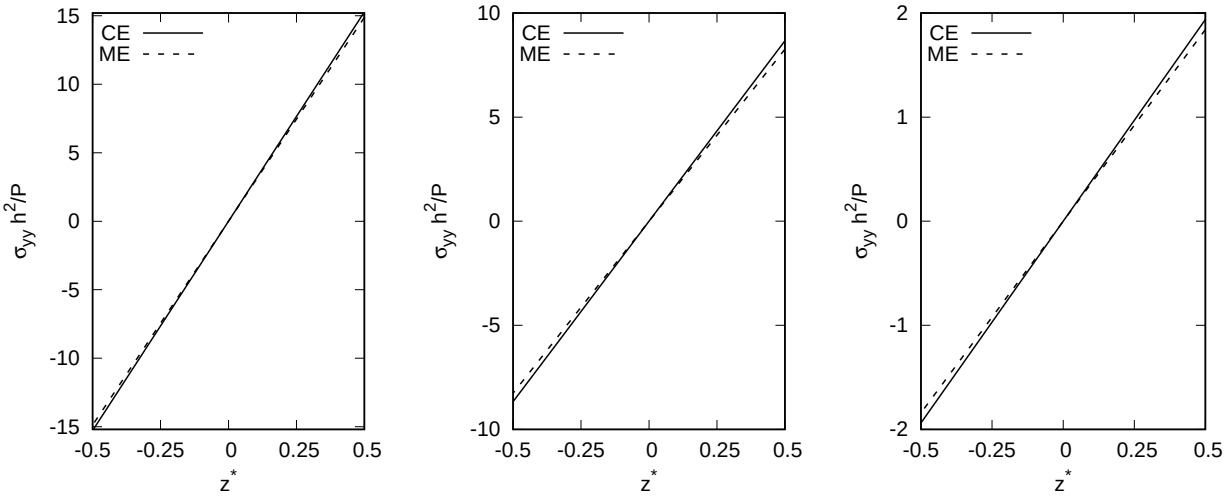

(a) y=0.1L (b) y=0.5L (c) y=0.9L

Figure 6: Distributions of the axial stress σ_{YY} h^2/P component adopting both CE and ME solutions along the thickness ($z^* = z/h$) of the beam. 1L9 LE model. $\dfrac{\alpha}{E} = 10^{-2}$, $\dfrac{\gamma}{E} = \dfrac{\epsilon}{E} = 2.5 \times 10^{-4}$.

ME solution is always lower than the ones from the CE solution, proving that a portion of the energy coming from the external force is absorbed by the work of the micro-rotations. Shear stress, σ_{YZ} and the σ_{ZY} components distributions from CE and ME along the beam thickness at the mid-span beam cross-section, $y = 0.5L$, are depicted in Fig. 7. For their evaluation, 1L16 LE cross-section model was used, instead of the 1L9 adopted for the calculation of the displacement, micro-rotation and the axial component of the stress. The reason is that the L9 model cannot accurately describe the quadratic distribution of the shear stress, so the adoption of a cubic interpolation, provided by a L16 LE, is mandatory, see [38, 41].

4.2 Effect of micropolar mechanical properties

In this section, the influence of the additional micropolar material parameters on the response of beam structures is addressed. The geometric, material and loading conditions are the same as in the previous analysis case. The elastic constants E and ν are taken as constant, while varying the micropolar parameters α, γ and ϵ. In the first analysis, the α parameter was varying, whereas γ and ϵ were fixed. The results are shown in Fig. 8, which gives the value of the ratio between the transverse displacement from CE and ME over the logarithmic value of the α parameter. When the value of the parameter decreases, the ratio increases. So, the lower is α, the closer is the solution between the two elasticity theories. On the contrary, increasing the value of the α parameter, the difference increases as well. Figure 9 shows the influence of the values of parameters γ and ϵ. As in the previous case, the ratio between the transverse displacement components from CE and ME is shown, over the values of the two additional material micropolar parameters. The trend is similar to the one shown in the previous figure. Finally, note that the effect of the variation of ϵ and γ is more evident than the variation of α. As a further analysis, the influence of the length of the beam was evaluated. Figure 10 shows the trend of the percentage difference between CE and ME for very short to long beams. The cross-section geometry changes every analysis according to the

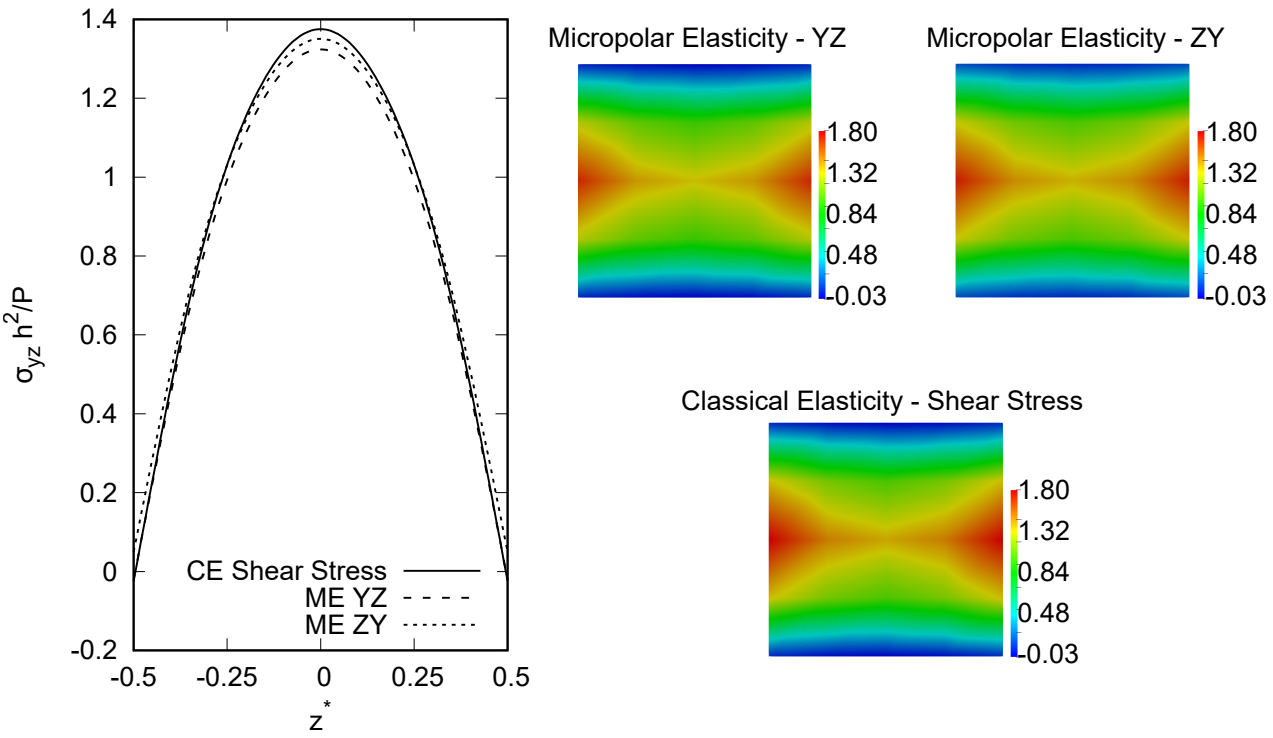

(a) y=0.5L

Figure 7: Trend of the transverse stress $\sigma_{YZ}\ h^2/P$ component adopting both CE and ME solutions along the thickness ($z^* = z/h$). 1L9 LE beam model. $\frac{\alpha}{E} = 10^{-2}$, $\frac{\gamma}{E} = \frac{\epsilon}{E} = 2.5 \times 10^{-4}$.

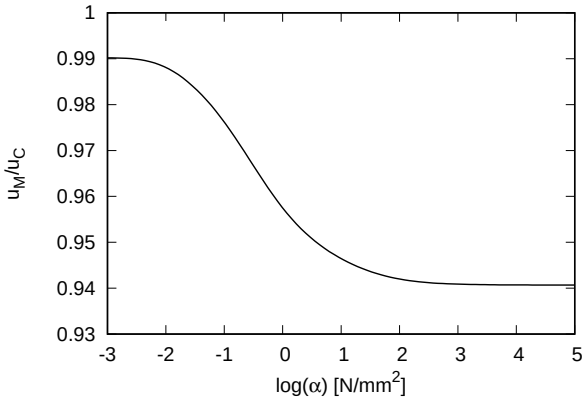

Figure 8: Influence of α on the static response of the cantilever beam.

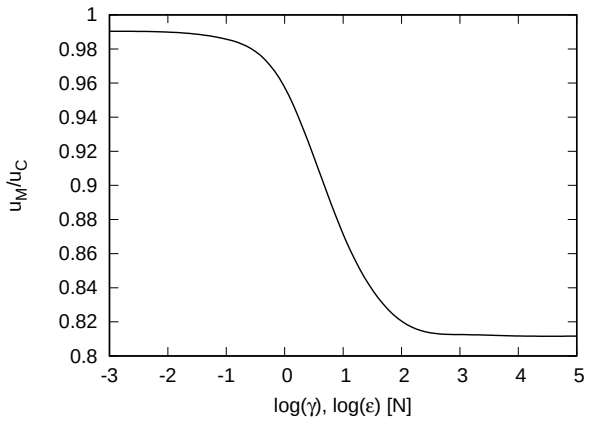

Figure 9: Influence of γ and ϵ on the static response of the cantilever beam.

length of the beam, keeping fixed the value of the parameter $\frac{L}{\sqrt{\frac{I}{A}}} = 10$. From the results shown in the figure, it is clear that the length of the beam has a strong influence on the static solution of the ME, that has higher importance when the scale of the beam is low.

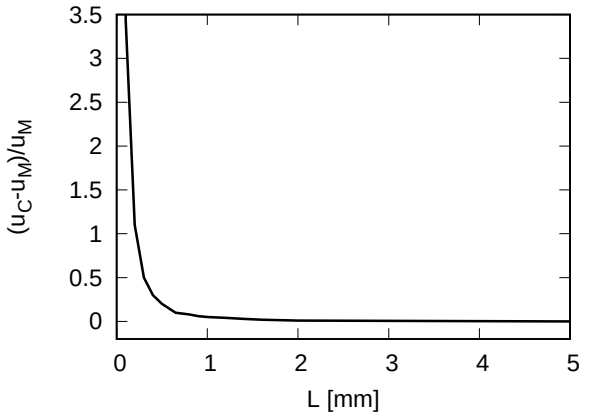

Figure 10: Influence of the length of the beam on the static response of the cantilever beam.

4.3 Human bone specimen

The following case deals with the analysis of a human bone specimen. The geometric and material properties come from the work of Yang and Lakes [20] and Lakes [42]. The human bone specimen selected in this case was modeled as a cylinder with a circular cross-section, which can be seen in Fig.11(a). The bone is made by a material with Young modulus $E =$ 14.1 GPa, $G = 4000$ GPa, $\gamma = 2487$ N, $\epsilon = 0$ N and $\alpha = 7428$ N/mm^2. The structure is subjected to clamped-free boundary condition and undergoes a transverse load. The diameter d is equal to 7 mm, and the total length of the bone is 53.4 mm. 12L9 Lagrange polynomials were adopted to discretize the cross-section, as displayed in Fig.11(b), along with the pattern of the points. Displacement on the z-direction and micro-rotation of the middle point of the cross-section, shown in Fig. 11(b), are given in Figure 12. Figure 12(a) compares the displacement calculated with both CE and ME over the beam axis coordinate. The percentage difference between the two solutions calculated at the tip of the beam is 8.2%, that is higher

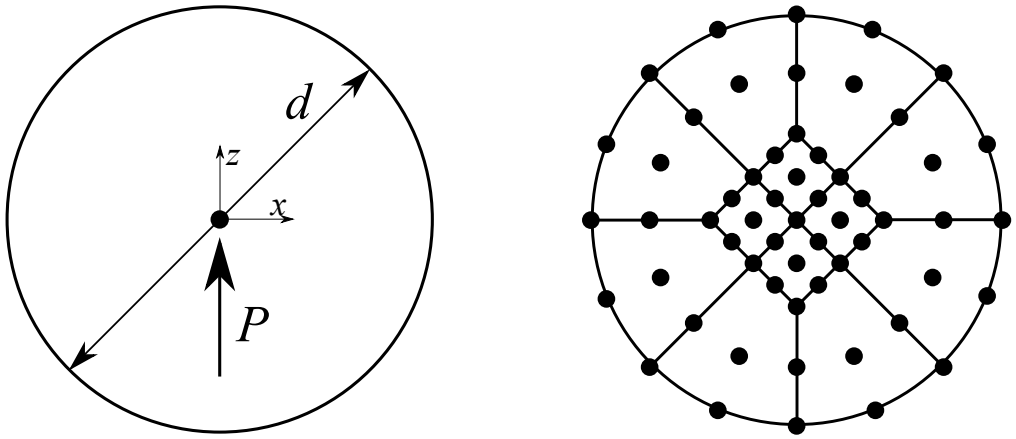

(a) (b)

Figure 11: Geometric properties, loading condition (a) and LE cross-section model (b) for the human bone specimen analysis case.

than the ones from the previous cases described in the previous sections. This behavior proves how a micropolar approach describes the behavior of the human bone better than the CE, as already stated by the reference paper. Figure 12(b) shows the value of the micro-rotation of the same point over the beam axis coordinate. Finally, an analysis of the force stress is given

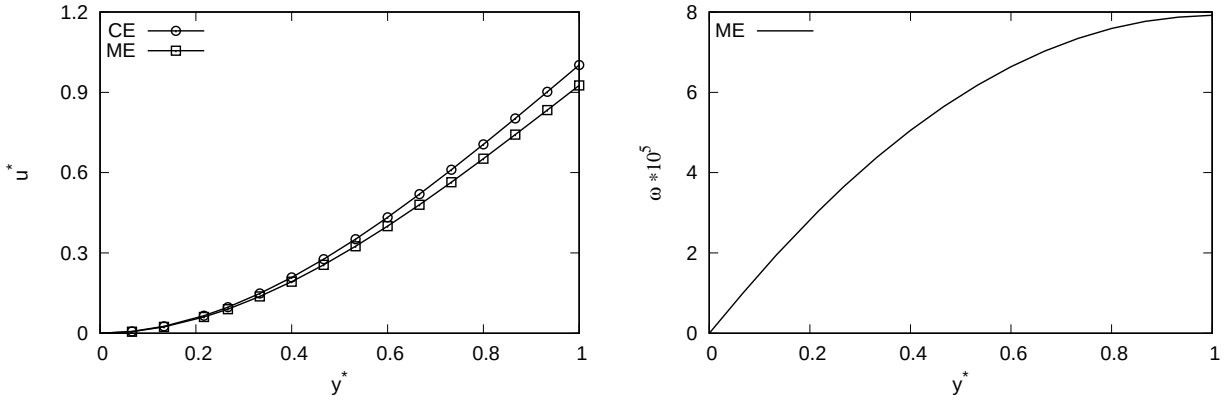

(a) (b)

Figure 12: Non-dimensional displacement ($u^* = \dfrac{3EILu(y)}{FAL^2}$) over non-dimensional coordinate ($y^* = \dfrac{y}{L}$) (a) and micro-rotations [rad] over non-dimensional coordinate (b). Present ME results are compared to the ones using CE. $E = 14.1$ GPa, $G = 4000$ GPa, $\gamma = 2487$ N, $\epsilon = 0$ N and $\alpha = 7428\ N/mm^2$.

hereafter. Figure 13 shows the normal stress $\sigma_{YY}\ h^3/PL$ component over the thickness of the beam for three cross-sections at 0.1 L, 0.5 L and 0.9 L. The figure shows a similar trend than in the previous cases, and it shows a very slight difference between the two solutions. Finally, Fig. 14 show the transverse $\sigma_{YZ}\ h^2/P$ component over the thickness at the middle cross-sections of the beam. The difference between the solutions is mainly at the center of the beam, where the σ_{YZ} and the σ_{ZY} components reach lower values than the shear stress calculated with the CE.

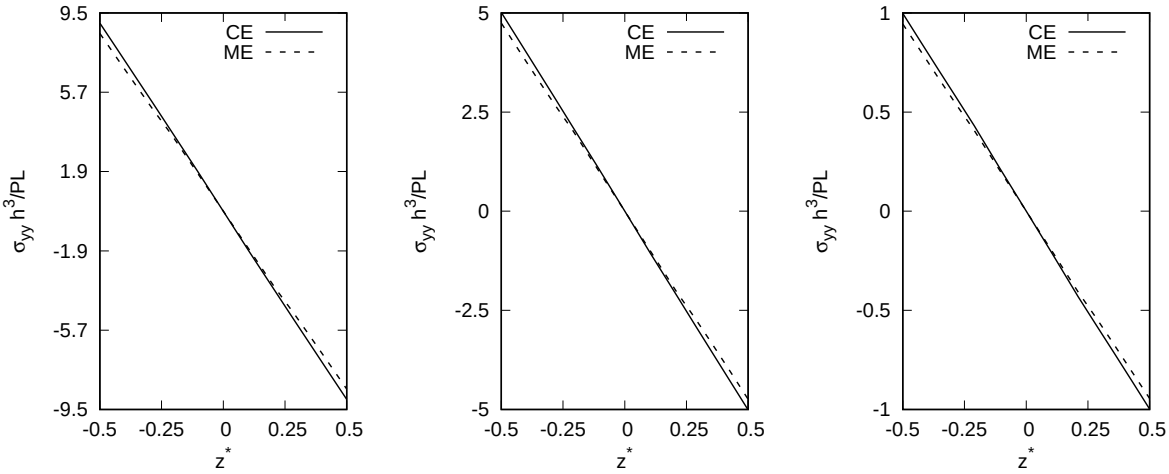

(a) y=0.1L (b) y=0.5L (c) y=0.9L

Figure 13: Trend of the axial stress $\sigma_{YY}\ h^2/P$ component adopting both CE and ME solutions along the thickness ($z^* = z/h$). $E = 14.1$ GPa, $G = 4000$ GPa, $\gamma = 2487$ N, $\epsilon = 0$ N and $\alpha = 7428\ N/mm^2$.

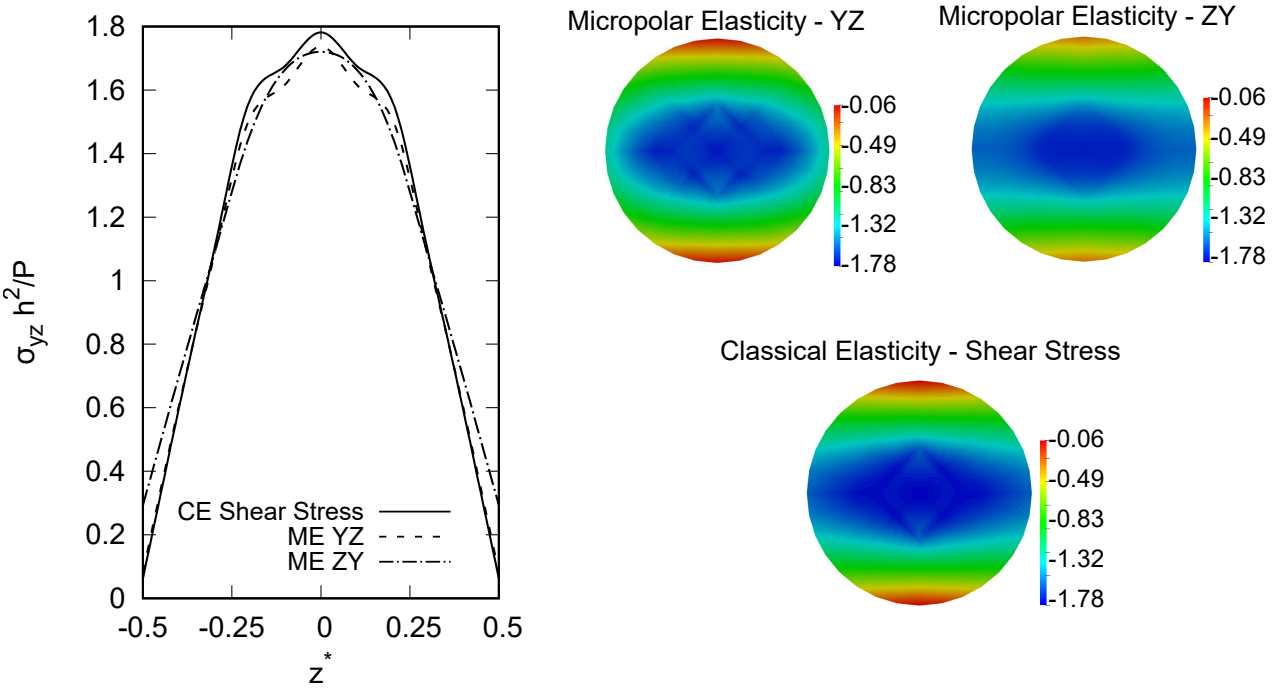

(a) y=0.5L

Figure 14: Trend of the transverse stress $\sigma_{YZ}\ h^2/P$ component adopting CE (a) and both CE and ME (b) over the thickness ($z^* = z/h$), at $y = L/2$. $E = 14.1$ GPa, $G = 4000$ GPa, $\gamma = 2487$ N, $\epsilon = 0$ N and $\alpha = 7428\ N/mm^2$.

5 Conclusions

A unified theory of structures based on Micropolar Elasticity (ME) has been proposed in this work. This theory has been developed in the framework of the Carrera Unified Formulation (CUF), which allows the 3D generalized displacements to be expressed as an arbitrary expansion of the primary variables. The ME can overcome the problems deriving from the adoption of Classical Elasticity (CE), such as the identification of local and size-effects, with the introduction of the micro-rotation vector as an unknown for every particle of the structure and four additional material parameters. The results demonstrate the validity of the proposed approach, trough a comparison with literature results, both in terms of displacements and micro-rotations. Stress distributions are considered as well, to compare the results between CE and ME. An analysis of the influence of the material parameters and the length of the beam has been conducted, highlighting the importance of adopting the ME. Finally, the adoption of ME for the analysis of a human bone specimen has been discussed, highlighting the differences between CE and ME.

References

[1] L. Euler. *De Curvis Elasticis, Additamentum I to his Methodus Inveniendi Lineas Curvas Maximi Minimive Proprietate Gaudentes*. Lausanne and Geneva, 1744.

[2] S. P. Timoshenko. On the transverse vibrations of bars of uniform cross-section. *The London, Edinburgh, and Dublin Philosophical Magazine and Journal of Science*, 43(253):125–131, 1922.

[3] C. A. Coulomb. Recherches théoriques et expérimentales sur la force de torsion et sur l'élasticité des fils de métal. *Histoire de l'Académie Royale des Sciences*, pages 229–269.

[4] B. de Saint-Venant. Mémoire sur la torsion des prismes. *Mémoires des Savants étrangers*, 14:233–560, 1855.

[5] T. C. Kennedy. Modeling failure in notched plates with micropolar strain softening. *Composite structures*, 44(1):71–79, 1999.

[6] L. Xiaodong, B. Bhushan, K. Takashima, C.-W. Baek, and Y.-K. Kim. Mechanical characterization of micro/nanoscale structures for mems/nems applications using nanoindentation techniques. *Ultramicroscopy*, 97(1-4):481–494, 2003.

[7] A. W. McFarland and J. S. Colton. Role of material microstructure in plate stiffness with relevance to microcantilever sensors. *Journal of Micromechanics and Microengineering*, 15(5):1060, 2005.

[8] D. Lam, F. Yang, A. Chong, J. Wang, and P. Tong. Experiments and theory in strain gradient elasticity. *Journal of the Mechanics and Physics of Solids*, 51(8):1477–1508, 2003.

[9] R. H. J. d Peerlings, R. De Borst, W. A. M. Brekelmans, and M. G. D. Geers. Localisation issues in local and nonlocal continuum approaches to fracture. *European Journal of Mechanics-A/Solids*, 21(2):175–189, 2002.

[10] I. A. Kunin. *Elastic media with microstructure I: One-Dimensional Models*, volume 26. Springer Series in Solid State Sciences, 1982.

[11] I. A. Kunin. *Elastic Media with Microstructure II: Three-dimensional Models*, volume 44. Springer Series in Solid State Sciences, 1983.

[12] G. A. Maugin and A. V. Metrikine. *Mechanics of generalized continua*. Springer, 2010.

[13] W. Voigt. *Theoretische studien über die elasticitätsverhältnisse der krystalle*. Königliche Gesellschaft der Wissenschaften zu Göttingen, 1887.

[14] E. Cosserat and F. Cosserat. *Théorie des corps déformables*. A. Hermann et fils, Paris, 1909.

[15] A. C. Eringen. Linear theory of micropolar elasticity. *Journal of Mathematics and Mechanics*, pages 909–923, 1966.

[16] A. C. Eringen. *Microcontinuum field theories I: Foundations and solids*. Springer Science & Business Media, 1999.

[17] A. C. Eringen. *Microcontinuum field theories II: Fluent media, 2001*. Springer Science & Business Media, 2001.

[18] W. Nowacki. *Theory of asymmetric elasticity*. Oxford, UK, 1986.

[19] W. Nowacki. *Theory of micropolar elasticity*. Number 25. Springer, 1972.

[20] J. F. C. Yang and R. S. Lakes. Experimental study of micropolar and couple stress elasticity in compact bone in bending. *Journal of Biomechanics*, 15(2):91–98, 1982.

[21] R. S. Lakes, S. Nakamura, J. C. Behiri, and W. Bonfield. Fracture mechanics of bone with short cracks. *Journal of Biomechanics*, 23(10):967–975, 1990.

[22] R. S. Lakes. Size effects and micromechanics of a porous solid. *Journal of Materials Science*, 18(9):2572–2580, 1983.

[23] S. Hassanpour and G. R. Heppler. Micropolar elasticity theory: a survey of linear isotropic equations, representative notations, and experimental investigations. *Mathematics and Mechanics of Solids*, 22(2):224–242, 2017.

[24] F.-Y. Huang, B.-H. Yan, J.-L. Yan, and D.-U. Yang. Bending analysis of micropolar elastic beam using a 3-d finite element method. *International Journal of Engineering Science*, 38(3):275–286, 2000.

[25] S. Ramezani, R. Naghdabadi, and S. Sohrabpour. Analysis of micropolar elastic beams. *European Journal of Mechanics-A/Solids*, 28(2):202–208, 2009.

[26] S. Hassanpour and G. R. Heppler. Comprehensive and easy-to-use torsion and bending theories for micropolar beams. *International Journal of Mechanical Sciences*, 114:71–87, 2016.

[27] V. V. Zozulya. Higher order theory of micropolar plates and shells. *ZAMM-Journal of Applied Mathematics and Mechanics/Zeitschrift für Angewandte Mathematik und Mechanik*, 98(6):886–918, 2018.

[28] V. V. Zozulya. Micropolar curved rods. 2-D, high order, Timoshenko's and Euler-Bernoulli models. *Curved and Layered Structures*, 4(1):104–118, 2017.

[29] E. Carrera and A. Varello. Dynamic response of thin-walled structures by variable kinematic one-dimensional models. *Journal of Sound and Vibration*, 331(24):5268–5282, 2012.

[30] F. A. Fazzolari and E. Carrera. Accurate free vibration analysis of thermo-mechanically pre/post-buckled anisotropic multilayered plates based on a refined hierarchical trigonometric ritz formulation. *Composite Structures*, 95:381–402, 2013.

[31] A. Pagani and E. Carrera. Unified formulation of geometrically nonlinear refined beam theories. *Mechanics of Advanced Materials and Structures*, 25(1):15–31, 2018.

[32] A. Pagani and E. Carrera. Large-deflection and post-buckling analyses of laminated composite beams by carrera unified formulation. *Composite Structures*, 170:40–52, 2017.

[33] E. Carrera and A. Pagani. Free vibration analysis of civil engineering structures by component-wise models. *Journal of Sound and Vibration*, 333(19):4597–4620, 2014.

[34] E. Carrera, M. Petrolo, and A. Varello. Advanced beam formulations for free-vibration analysis of conventional and joined wings. *Journal of Aerospace Engineering*, 25(2):282–293, 2011.

[35] F. Miglioretti and E. Carrera. Application of a refined multi-field beam model for the analysis of complex configurations. *Mechanics of Advanced Materials and Structures*, 22(1-2):52–66, 2015.

[36] E. Carrera and V.V. Zozulya. Carrera unified formulation (cuf) for the micropolar beams: Analytical solutions. *Mechanics of Advanced Materials and Structures*, pages 1–25, 2019.

[37] E. Carrera, M. Cinefra, M. Petrolo, and E. Zappino. *Finite element analysis of structures through unified formulation*. John Wiley & Sons, 2014.

[38] E. Carrera and M. Petrolo. Refined beam elements with only displacement variables and plate/shell capabilities. *Meccanica*, 47(3):537–556, 2012.

[39] E. Carrera, M. Cinefra, A. Lamberti, and M. Petrolo. Results on best theories for metallic and laminated shells including layer-wise models. *Composite Structures*, 126:285–298, 2015.

[40] K.J. Bathe. *Finite element procedure*. Prentice hall, Upper Saddle River, New Jersey, USA, 1996.

[41] E. Carrera, M. Cinefra, M. Petrolo, and E. Zappino. Comparisons between 1d (beam) and 2d (plate/shell) finite elements to analyze thin walled structures. *Aerotecnica Missili & Spazio*, 93(1-2):3–16, 2014.

[42] R. Lakes. Experimental micro mechanics methods for conventional and negative poissons ratio cellular solids as cosserat continua. *Journal of Engineering Materials and Technology*, 113(1):148–155, 1991.

Appendix A Components of the secant stiffness matrix

$$\mathbf{K}^{\tau sij}_{uuxx} = C_{11}\int_\Omega F_{\tau,x}\,F_{s,x}d\Omega\int_L N_i\,N_j dL + C^M_{55}\int_\Omega F_{\tau,z}\,F_{s,z}d\Omega\int_L N_i\,N_j dL + C^M_{44}\int_\Omega F_\tau\,F_s d\Omega\int_L N_{i,y}\,N_{j,y}dL$$

$$\mathbf{K}^{ij\tau s}_{uuxy} = C_{12}\int_\Omega F_\tau\,F_{s,x}d\Omega\int_L N_{i,y}\,N_j dL + C^{MT}_{44}\int_\Omega F_{\tau,x}\,F_s d\Omega\int_L N_i\,N_{j,y}dL$$

$$\mathbf{K}^{ij\tau s}_{uuxz} = C^{MT}_{55}\int_\Omega F_{\tau,x}\,F_{s,z}d\Omega\int_L N_i\,N_j dL + C_{13}\int_\Omega F_{\tau,z}\,F_{s,x}d\Omega\int_L N_i\,N_j dL$$

$$\mathbf{K}^{ij\tau s}_{uuyx} = C^{MT}_{44}\int_\Omega F_{\tau,z}\,F_{s,x}d\Omega\int_L N_{i,y}\,N_j dL + C_{12}\int_\Omega F_{\tau,x}\,F_s d\Omega\int_L N_i\,N_{j,y}dL$$

$$\mathbf{K}^{\tau sij}_{uuyy} = C^M_{44}\int_\Omega F_{\tau,x}\,F_{s,x}d\Omega\int_L N_i\,N_j dL + C^M_{66}\int_\Omega F_{\tau,z}\,F_{s,z}\,N_i\,N_j d\Omega\int_L + C_{22}\int_\Omega F_\tau\,F_s d\Omega\int_L N_{i,y}\,N_{j,y}dL$$

$$\mathbf{K}^{ij\tau s}_{uuyz} = C^{MT}_{66}\int_\Omega F_\tau\,F_{s,z}d\Omega\int_L N_{i,y}\,N_j dL + C_{23}\int_\Omega F_{\tau,z}\,F_s d\Omega\int_L N_i\,N_{j,y}dL$$

$$\mathbf{K}^{ij\tau s}_{uuzx} = C_{13}\int_\Omega F_{\tau,x}\,F_{s,z}d\Omega\int_L N_i\,N_j dL + C^{MT}_{55}\int_\Omega F_{\tau,z}\,F_{s,x}d\Omega\int_L N_i\,N_j dL$$

$$\mathbf{K}^{ij\tau s}_{uuzy} = C_{23}\int_\Omega F_\tau\,F_{s,z}d\Omega\int_L N_{i,y}\,N_j dL + C^{MT}_{66}\int_\Omega F_{\tau,z}\,F_s d\Omega\int_L N_i\,N_{j,y}dL$$

$$\mathbf{K}^{\tau sij}_{uuzz} = C^{MT}_{55}\int_\Omega F_{\tau,x}\,F_{s,x}d\Omega\int_L N_i\,N_j dL + C_{33}\int_\Omega F_{\tau,z}\,F_{s,z}d\Omega\int_L N_i\,N_j dL + C^{MT}_{66}\int_\Omega F_\tau\,F_s d\Omega\int_L N_{i,y}\,N_{j,y}dL$$

$$\mathbf{K}^{ij\tau s}_{u\omega xx} = 0$$

$$\mathbf{K}^{ij\tau s}_{u\omega xy} = -C^M_{55}\int_\Omega F_\tau\,F_{s,z}d\Omega\int_L N_i\,N_j dL + C^{MT}_{55}\int_\Omega F_\tau\,F_{s,z}d\Omega\int_L N_i\,N_j dL$$

$$\mathbf{K}^{ij\tau s}_{u\omega xz} = C^M_{44}\int_\Omega F_\tau\,F_s d\Omega\int_L N_i\,N_{j,y}dL - C^{MT}_{44}\int_\Omega F_\tau\,F_s d\Omega\int_L N_i\,N_{j,y}dL$$

$$\mathbf{K}^{ij\tau s}_{u\omega yx} = C^M_{66}\int_\Omega F_\tau\,F_{s,z}d\Omega\int_L N_i\,N_j dL - C^{MT}_{66}\int_\Omega F_\tau\,F_{s,z}d\Omega\int_L N_i\,N_j dL$$

$$\mathbf{K}^{ij\tau s}_{u\omega yy} = 0$$

$$\mathbf{K}^{ij\tau s}_{u\omega yz} = C^{MT}_{44}\int_\Omega F_\tau\,F_{s,x}d\Omega\int_L N_i\,N_j dL - C^M_{44}\int_\Omega F_\tau\,F_{s,x}d\Omega\int_L N_i\,N_j dL$$

$$\mathbf{K}^{ij\tau s}_{u\omega zx} = -C^{M}_{66}\int_{\Omega} F_{\tau}\, F_{s} d\Omega \int_{L} N_i\, N_{j,y} dL + C^{MT}_{66}\int_{\Omega} F_{\tau}\, F_{s} d\Omega \int_{L} N_i\, N_{j,y} dL$$

$$\mathbf{K}^{ij\tau s}_{u\omega zy} = C^{M}_{55}\int_{\Omega} F_{\tau}\, F_{s_{,x}} d\Omega \int_{L} N_i\, N_{j} dL - C^{MT}_{55}\int_{\Omega} F_{\tau}\, F_{s_{,x}} d\Omega \int_{L} N_i\, N_{j} dL$$

$$\mathbf{K}^{ij\tau s}_{u\omega zz} = 0$$

$$\mathbf{K}^{ij\tau s}_{\omega uxx} = 0$$

$$\mathbf{K}^{ij\tau s}_{\omega uxy} = C^{M}_{66}\int_{\Omega} F_{s}\, F_{t_{,z}} d\Omega \int_{L} N_i\, N_{j} dL - C^{MT}_{66}\int_{\Omega} F_{s}\, F_{t_{,z}} d\Omega \int_{L} N_i\, N_{j} dL$$

$$\mathbf{K}^{ij\tau s}_{\omega uxz} = -C^{M}_{66}\int_{\Omega} F_{s}\, F_{t} d\Omega \int_{L} N_{i_{,y}}\, N_{j} dL + C^{MT}_{66}\int_{\Omega} F_{s}\, F_{t} d\Omega \int_{L} N_{i_{,y}}\, N_{j_{,y}} dL$$

$$\mathbf{K}^{ij\tau s}_{\omega uyx} = -C^{M}_{55}\int_{\Omega} F_{s}\, F_{t_{,z}} d\Omega \int_{L} N_i\, N_{j} dL + C^{MT}_{55}\int_{\Omega} F_{s}\, F_{t_{,z}} d\Omega \int_{L} N_i\, N_{j} dL$$

$$\mathbf{K}^{ij\tau s}_{\omega uyy} = 0$$

$$\mathbf{K}^{ij\tau s}_{\omega uyz} = C^{M}_{55}\int_{\Omega} F_{s}\, F_{t_{,x}} d\Omega \int_{L} N_i\, N_{j} dL - C^{MT}_{55}\int_{\Omega} F_{s}\, F_{t_{,x}} d\Omega \int_{L} N_i\, N_{j} dL$$

$$\mathbf{K}^{ij\tau s}_{\omega uzx} = C^{M}_{44}\int_{\Omega} F_{s}\, F_{t} d\Omega \int_{L} N_{i_{,y}}\, N_{j} dL - C^{MT}_{44}\int_{\Omega} F_{s}\, F_{t} d\Omega \int_{L} N_{i_{,y}}\, N_{j} dL$$

$$\mathbf{K}^{ij\tau s}_{\omega uzy} = -C^{M}_{44}\int_{\Omega} F_{s}\, F_{t_{,x}} d\Omega \int_{L} N_i\, N_{j} dL + C^{MT}_{44}\int_{\Omega} F_{s}\, F_{t_{,x}} d\Omega \int_{L} N_i\, N_{j} dL$$

$$\mathbf{K}^{ij\tau s}_{\omega uzz} = 0$$

$$\mathbf{K}^{ij\tau s}_{\omega\omega xx} = 2C^{M}_{66}\int_{\Omega} F_{s}\, F_{t} d\Omega \int_{L} N_i\, N_{j} dL - 2C^{MT}_{66}\int_{\Omega} F_{s}\, F_{t} d\Omega \int_{L} N_i\, N_{j} dL +$$

$$A_{11}\int_{\Omega} F_{\tau_{,x}}\, F_{s_{,x}} d\Omega \int_{L} N_i\, N_{j} dL + A_{55}\int_{\Omega} F_{\tau_{,z}}\, F_{s_{,z}} d\Omega \int_{L} N_i\, N_{j} dL + A_{44}\int_{\Omega} F_{\tau}\, F_{s} d\Omega \int_{L} N_{i_{,y}}\, N_{j_{,y}} dL$$

$$\mathbf{K}^{ij\tau s}_{uuxz} = A_{12}\int_{\Omega} F_{\tau}\, F_{s_{,x}} d\Omega \int_{L} N_{i,y}\, N_{j} dL + A^{MT}_{44}\int_{\Omega} F_{\tau_{,x}}\, F_{s} d\Omega \int_{L} N_i\, N_{j_{,y}} dL$$

$$\mathbf{K}^{ij\tau s}_{uuxz} = A^{MT}_{55}\int_{\Omega} F_{\tau_{,x}}\, F_{s_{,z}} d\Omega \int_{L} N_i\, N_{j} dL + A_{13}\int_{\Omega} F_{\tau_{,z}}\, F_{s_{,x}} d\Omega \int_{L} N_i\, N_{j} dL$$

$$\mathbf{K}^{ij\tau s}_{uuyx} = A^{MT}_{44}\int_{\Omega} F_{\tau}\, F_{s_{,x}} d\Omega \int_{L} N_{i,y}\, N_{j} dL + A_{12}\int_{\Omega} F_{\tau_{,x}}\, F_{s} d\Omega \int_{L} N_i\, N_{j_{,y}} dL$$

$$\mathbf{K}^{ij\tau s}_{\omega\omega xx} = 2C^{M}_{55}\int_{\Omega} F_{s}\, F_{t} d\Omega \int_{L} N_i\, N_{j} dL - 2C^{MT}_{55}\int_{\Omega} F_{s}\, F_{t} d\Omega \int_{L} N_i\, N_{j} dL +$$

$$A_{44}\int_{\Omega} F_{\tau,x}\,F_{s,x}d\Omega\int_{L} N_i\,N_j dL + A_{66}\int_{\Omega} F_{\tau,z}\,F_{s,z}d\Omega\int_{L} N_i\,N_j dL + A_{22}\int_{\Omega} F_{\tau}\,F_{s}d\Omega\int_{L} N_{i,y}\,N_{j,y}dL$$

$$\mathbf{K}^{ij\tau s}_{uuyz} = A^{MT}_{66}\int_{\Omega} F_{\tau}\,F_{s,z}d\Omega\int_{L} N_{i,y}\,N_j dL + A_{23}\int_{\Omega} F_{\tau,z}\,F_{s}d\Omega\int_{L} N_i\,N_{j,y}dL$$

$$\mathbf{K}^{ij\tau s}_{uuzx} = A_{13}\int_{\Omega} F_{\tau,x}\,F_{s,z}d\Omega\int_{L} N_i\,N_j dL + A^{MT}_{55}\int_{\Omega} F_{\tau,z}\,F_{s,x}d\Omega\int_{L} N_i\,N_j dL$$

$$\mathbf{K}^{ij\tau s}_{uuzy} = A^{MT}_{66}\int_{\Omega} F_{\tau,z}\,F_{s}d\Omega\int_{L} N_i\,N_{j,y} dL + A_{23}\int_{\Omega} F_{\tau}\,F_{s,z}d\Omega\int_{L} N_{i,y}\,N_j dL$$

$$\mathbf{K}^{ij\tau s}_{\omega\omega xx} = 2C^{M}_{44}\int_{\Omega} F_{s}\,F_{t}d\Omega\int_{L} N_i\,N_j dL - 2C^{MT}_{44}\int_{\Omega} F_{s}\,F_{t}d\Omega\int_{L} N_i\,N_j dL +$$

$$A_{55}\int_{\Omega} F_{\tau,x}\,F_{s,x}d\Omega\int_{L} N_i\,N_j dL + A_{33}\int_{\Omega} F_{\tau,z}\,F_{s,z}d\Omega\int_{L} N_i\,N_j dL + A_{66}\int_{\Omega} F_{\tau}\,F_{s}d\Omega\int_{L} N_{i,y}\,N_{j,y}dL$$